PERK inhibition with GSK2606414 in zebrafish evokes developmental defects consistent with Wolcott-Rallison syndrome phenotypes

Liliana M. Almeida[a,b], Leonor Pereira Lima [a,b], Nuno A. S. Oliveira [a,b], Rui F. O. Silva [a,b], Bruno Sousa [a,b], José Bessa [c,d], Brígida R. Pinho [a,b], Jorge M. A. Oliveira [a,b,*]

[a]UCIBIO, Applied Molecular Biosciences Unit, Mitochondria and Neurobiology Lab, Faculdade de Farmácia, Universidade do Porto, 4050-313 Porto, Portugal

[b]i4HB, Institute for Health and Bioeconomy, Universidade do Porto, 4050-313 Porto, Portugal

[c]IBMC, Instituto de Biologia Molecular e Celular, Universidade do Porto, 4200-135 Porto, Portugal

[d]i3S, Instituto de Investigação e Inovação em Saúde, Universidade do Porto, 4200-135 Porto, Portugal

***Corresponding author:**

Jorge M. A. Oliveira (jorgemao@ff.up.pt)

Departamento de Ciências do Medicamento, Laboratório de Farmacologia, Faculdade de Farmácia, Universidade do Porto

Rua de Jorge Viterbo Ferreira, 228, 4050-313 Porto, Portugal | Tel. +351 220428610

Author's ORCID:

Liliana M. Almeida - 0000-0003-1042-511X

Leonor Pereira Lima - 0000-0003-3454-1799

Nuno A. S. Oliveira - 0000-0002-0735-8457

Rui F. O. Silva - 0000-0001-5470-778X

Bruno Sousa - 0000-0002-3995-8545

José Bessa - 0000-0002-8591-7138

Brígida R. Pinho - 0000-0002-1627-6795

Jorge M. A. Oliveira - 0000-0002-6040-5355

Abbreviations List:

2-NBDglucose, (2-(7-Nitro-2,1,3-benzoxadiazol-4-yl)-D-glucosamine); ATF4, Activating Transcription Factor 4; CHOP, C/EBP homologous protein; dpf, days post-fertilization; dTC, d-tubocurarine; eIF2α, eukaryotic translation initiation factor 2α; ER, Endoplasmic reticulum; hfp, hours post-fertilization; GSK, GSK2606414; ISR, Integrated Stress Response; NPH, Nikon-Prior-Hamamatsu; PERK, Protein kinase R-like ER kinase; WRS, Wolcott-Rallison Syndrome

Running Title: Zebrafish PERK in developmental diseases

Abstract

Background PERK (EIF2AK3) is an endoplasmic reticulum stress kinase whose loss of function disturbs human development, leading to skeletal dysplasia and permanent neonatal diabetes, as observed in the Wolcott-Rallison Syndrome (WRS). The lack of effective, less invasive therapies for developmental diseases highlights the need for animal models that replicate complex pathological phenotypes, while allowing scalable drug screening. Zebrafish, with their high fecundity and rapid development, facilitate efficient *in vivo* drug testing.

Methods We aimed to assess the potential of zebrafish for studying PERK function and its pharmacological modulation, particularly as a model for developmental diseases like WRS. Bioinformatic analyses assessed the similarity between human and zebrafish PERK. Increasing concentrations of GSK2606414 were used to inhibit PERK. A combination of behavioural and functional assays evaluated the effects of GSK2606414 on zebrafish skeletal, neuromuscular, and cardiac development. Fluorescence microscopy in transgenic zebrafish expressing fluorescent pancreatic markers and a glucose probe assessed the diabetic-like phenotype.

Results We found high similarity between human and zebrafish PERK, along with bioactivity of the PERK inhibitor GSK2606414 in zebrafish. PERK inhibition evoked defects in WRS relevant parameters, such as growth and skeletal development, as well as neuromuscular and cardiac deficiencies, whereas parameters not associated with WRS like otolith area and eye/body ratio remained unaffected. Moreover, PERK inhibition decreased pancreatic β cell mass and disrupted glucose homeostasis, indicating a diabetic phenotype.

Conclusion These findings evidence zebrafish's potential for studying PERK function and its pharmacological modulation in developmental disorders like WRS, aiding research on pathophysiology and experimental treatments.

Keywords: developmental diseases; metabolic diseases; model organism; zebrafish; PERK; Wolcott-Rallison syndrome

68 **1. Introduction**

69 Protein kinase RNA-like endoplasmic reticulum kinase (PERK) is an endoplasmic reticulum
70 (ER) membrane kinase that activates in response to disruptions in ER protein homeostasis
71 (proteostasis) by promoting a protective response, the integrated stress response (ISR). Upon
72 activation by stress, PERK phosphorylates eukaryotic translation initiation factor 2α (eIF2α)
73 that decreases global protein synthesis, alleviating nascent protein load (1) and boosts the
74 synthesis of transcription factors like activating transcription factor 4 (ATF4) and C/EBP
75 homologous protein (CHOP). These transcription factors regulate the expression of
76 chaperones, proteases and components of the autophagic pathway, thus contributing to
77 proteostasis maintenance (1). During development, protein synthesis plays a critical role in cell
78 division, differentiation, and the rapid growth of embryos (2), and PERK is essential for
79 detecting protein misfolding and adjusting protein synthesis to maintain proteostasis (3).

80 In humans, loss-of-function mutations in the *EIF2AK3* gene encoding for PERK cause a
81 rare (prevalence of <1/1 000 000; ORPHA:1667) autosomal recessive developmental disease
82 named Wolcott-Rallison Syndrome (WRS), with patients dying before 35 years of age (4).
83 WRS is mainly characterized by skeletal dysplasia and neonatal diabetes mellitus (5), but WRS
84 patients may also present broad symptomatology like motor neuropathy, intellectual deficit,
85 early neurodegeneration, and cardiac malformations (4). This broad symptomatology is likely
86 due to the widespread distribution of PERK, with several loss-of-function mutations totally or
87 partially abolishing its kinase activity (4, 6). Existing therapies for WRS patients include blood
88 glucose control with insulin pumping and transplant of liver/pancreas and kidney (7). The
89 scarcity of non-invasive and more effective therapeutic options for WRS patients highlights
90 the need for further therapeutic investigation, which requires efficient WRS models.

91 The currently available *in vivo* models for the developmental disease WRS are rodents
92 with PERK knock-out or loss-of-function mutations in PERK that exhibit the WRS hallmarks

93 – neonatal diabetes and skeletal dysplasia (8, 9) – and the broad-spectrum phenotypes – cardiac,
94 muscle and cognitive abnormalities (10-12). However, for large exploratory studies of new
95 therapeutics, there are efficiency advantages in using small vertebrates like zebrafish before
96 testing the most promising candidates in rodent models. Zebrafish are increasingly used to
97 develop disease models given their advantageous features: high fecundity, external
98 fertilization, and rapid formation of complete organs, making zebrafish ideal for investigating
99 developmental diseases and for rapid and scalable *in vivo* drug testing (13, 14). Previous studies
100 that targeted PERK in zebrafish, used either genetic (morpholino knockdown) or
101 pharmacological inhibition (15-17). In such studies, PERK inhibition with GSK2606414 was
102 used in zebrafish adults to study sleep regulation (15), and PERK inhibition with GSK2656157
103 or PERK knockdown was used to study redox regulation and neurogenesis in zebrafish
104 embryos (16, 17). To the best of our knowledge, there are no previous studies in zebrafish with
105 a primary focus on studying PERK function in developmental diseases, including WRS.
106 Here, we combined bioinformatic analyses, molecular biology techniques, behaviour,
107 and functional assays to assess the effects of pharmacological PERK inhibition in zebrafish.
108 We used transgenic zebrafish expressing pancreatic reporters and a fluorescent glucose probe
109 to assess diabetic-like phenotypes. We performed functional and structural microscopy to
110 assess skeletal, neuromuscular, and cardiac development. Our data show that zebrafish holds
111 potential as a model to study PERK function in developmental disorders, such as WRS.
112

113 ## 2. Material and Methods

114

115 ### 2.1 Drugs, solvents, and solutions

116 Stock solutions of the PERK inhibitor GSK2606414 (Merck Millipore, 516535) (15, 18), the
117 muscle relaxant D-tubocurarine (dTC; Sigma, T2379), and the anesthetic tricaine
118 methanesulfonate (0.02%; Sigma, E10521) were prepared in DMSO (Sigma, 276855) and
119 diluted in standard E3 medium (19). DMSO levels were kept under 0.2% (20).

120

121 ### 2.2 Zebrafish maintenance and husbandry

122 Adult AB strain zebrafish were supplied by the Interdisciplinary Centre of Marine and
123 Environmental Research (CIIMAR, Portugal), transgenic strains of zebrafish were obtained
124 from José Bessa's laboratory at the Institute for Research and Innovation in Health (i3s,
125 University of Porto, Portugal). Zebrafish adults were maintained at 28 ± 1°C on a 14 h:10 h
126 light:dark cycle (21, 22). Breeding pairs (1:1, male:female) were placed in breeding tanks on
127 the day before egg collection. Ninety minutes after starting the light period, eggs were
128 collected, and time point was recorded as 0 h post fertilization (hpf). **Ethic statement:**
129 Handling of zebrafish followed the European Directive 2010/63/EU and the Portuguese Law
130 (Decreto-Lei 113/2013). Experiments were performed according to the 3Rs principle by
131 reducing the number of animals used and using refined techniques that reduce animal suffering,
132 using procedures approved by the i3S Animal Welfare Body.

133

134 ### 2.3 Drug treatments

135 5 zebrafish/well were randomly distributed in 24-well plates (0.5 mL E3/well) and kept at 28
136 ± 1°C on a 14 h:10 h light: dark cycle throughout the assay. Zebrafish were continuously

137 exposed to GSK2606414 or solvent (DMSO) from 4 to 76 hpf and solutions were renewed
138 daily (21). dTC was incubated for 10 minutes before assays endpoint (≥ 15 zebrafish).
139

140 **2.4 Brightfield microscopy**

141 For brightfield microscopy, we used a stereomicroscope (Stemi DV4, Zeiss, Göttingen,
142 Germany) or an inverted microscope (Eclipse TE300, Nikon, Tokyo, Japan). The inverted
143 microscope was attached to a motorized stage (ProScan, Prior) and a CCD camera (ORCA-
144 ER, Hamamatsu), constituting a Nikon-Prior-Hamamatsu (NPH) imaging system that was
145 controlled by the open-source software Micro-Manager (v. 2.0; https://micro-manager.org):

146 2.4.1 ***Monitoring zebrafish development:*** Zebrafish were scored as normal,
147 abnormal, or dead; hatched (ruptured chorion and free tail movement) or unhatched at
148 28, 52 and 76 hpf. Death was ascertained according to OECD guideline 236 (23),
149 normal development as previously described (24), and abnormalities as cardiac and
150 skeletal (further into scoliosis, curly-up tail, or kyphosis). Dead zebrafish were removed
151 at each time point and only live ones were used in subsequent assays.

152 **2.4.2** ***Morphometric analysis:*** Zebrafish body length was measured from the tip of
153 the head (between the eyes) to the end of the tail (25) and trunk-tail angle was measured
154 at the intersection between the rostral (trunk) and caudal (tail) notochord at the level of
155 the anus (Figure 3 B).

156 2.4.3 ***Heartbeat and atrio-ventricular coordination:*** Heartbeats were counted in 4
157 zebrafish per condition, per experiment, during 20 s, at 72-80 hpf (26). Atrio-
158 ventricular coordination recordings were obtained with "Plot Z-axis profile" on ImageJ
159 after imaging zebrafish for 90 seconds at 12 frames per second.

160 2.4.4 ***Tail coilings:*** Spontaneous activity was measured at 28 hpf in glass bottom 96-
161 well plates where each zebrafish was imaged for 3 minutes at a frequency of 4.5 frames
162 per second and 2x2 or 4x4 binning (19).
163 **2.4.5** ***Birefringence analysis:*** 76 hpf zebrafish were anesthetized, immobilized on a
164 glass surface, oriented laterally, and illuminated with linearly polarized light (Screen-
165 Tech, ST-38). An orthogonal polarization filter was placed after the samples to block
166 directly transmitted light. Thus, only light whose polarization angle is affected by the
167 sample is collected by the NPH imaging system (27). Pixel intensity in the trunk region
168 was measured by selecting the region of interest with ImageJ software.
169
170 **2.5 Touch-evoked escape response**
171 At 76 hpf, at least 6 zebrafish/condition were submitted to 10 alternate touches to the head and
172 to the tail with 10 µL pipette tip with a recovery time of 30 seconds (28). Data are presented as
173 response rates in percentage of total touches.
174
175 **2.6 Fluorescent microscopy**
176 Zebrafish were imaged with the NPH system coupled to a monochromator (Polychrome II,
177 Photonics) as follows.
178 **2.6.1** ***2-NBDG labelling:*** 3 hours before 76 hpf end-point, zebrafish were incubated
179 with a fluorescent glucose analogue - 600 µM 2-NBDglucose (2-(7-Nitro-2,1,3-
180 benzoxadiazol-4-yl)-D-glucosamine) (Tebu-Bio,10-1459) (29, 30); and a positive
181 control for neuromast labelling - Mitotracker Deep Red (1 µM, Invitrogen, M22426,
182 labels polarized mitochondria in neuromasts) in 96 well plates (4 zebrafish /well). At
183 76 hpf, each zebrafish was anesthetized and imaged in a glass-bottom chamber. 2-
184 NBDglucose was excited at 475 nm and Mitotracker Deep Red at 650 nm for 1 second.

185 Emissions were collected using band pass filters (Chroma 69008 – ET –
186 ECFP/EYFP/mCherry) with a 10 × objective. Images of the entire fish were stitched
187 with the GNU image manipulation program (The GIMP Development Team, 2019;
188 https://www.gimp.org), before evaluation of anterior and posterior neuromasts (31).
189 **2.6.2** ***Transgenic zebrafish:*** Double transgenic zebrafish expressing GFP in insulin-
190 producing β cells and mCherry in somatostatin-producing δ cells (Tg(ins:GFP,
191 sst:mCherry)) or in elastase-producing cells (Tg(ins:GFP, ela:mCherry)) were kept in
192 24-well plates (5 zebrafish/plate) with E3 media. We used two pharmacological
193 approaches: 1) GSK2606414 exposure from 4 hpf (before the principal islet of
194 Langerhans is formed within the endocrine pancreas) to 28, 76 or 148 hpf; 2)
195 GSK2606414 exposure from 76 hpf (when the principal islet is already formed) to 148
196 hpf (32). At the final time point (28, 76 or 148 hpf) zebrafish were anesthetized by rapid
197 cooling on ice and fixed in 4% paraformaldehyde overnight. GFP was excited at 488
198 nm and mCherry was excited at 575 nm. Emissions were collected using band pass
199 filters (Chroma 59022 – EGFP/mCherry) with a 20 × objective. The area of GFP- or
200 mCherry-labelled pancreas in each image was assessed with the ImageJ software
201 (https://imagej.nih.gov/ij).
202
203 **2.8 Western blot**
204 24-27 zebrafish larvae were rinsed with ice-cold water twice before being placed in RIPA
205 buffer (50 mM Tris (NZYTech, MB01601), 150 mM NaCl (Merck, S9888), 1 mM EDTA
206 (Sigma-Aldrich, E6758), 1% IGEPAL CA-630 (Sigma-Aldrich, I3021), 1% sodium
207 deoxycholate (Sigma-Aldrich, D6750), 0.1% sodium dodecyl sulfate (Sigma-Aldrich, L3771)
208 supplemented with a protease and phosphatase inhibitor cocktail (Thermo Scientific, 78440).
209 After 3 freeze-thaw cycles, homogenization with Precellys Evolution (6800 rpm, 5 × 42 s with

210 37 s interval) and centrifugation at 12,000 × g (10 min, 4 °C), supernatant protein
211 concentrations were quantified by the Bradford method. 30 to 40 µg of protein extracts were
212 supplemented with Bolt LDS sample buffer (Invitrogen, B0007) and Bolt sample reducing
213 agent (Invitrogen, B0009), denatured at 95 ºC for 5 min, and loaded into 4–15% Mini-
214 PROTEAN TGX™ Precast Protein Gels (Biorad, 4561084), which were electrophoresed (125
215 and 200 V, 30 min) and wet-transferred to PVDF membranes (Millipore, IPVH00010)
216 overnight (30 V, 4ºC). Membranes were blocked (1 h, room temperature or overnight at 4ºC)
217 with 5% bovine serum albumin (BSA, NZYTech, MB04602) in PBS with 0.05% Tween 20
218 (PBST) and incubated with primary antibodies (Supplementary Table 1). After washing with
219 PBST, membranes were incubated with respective horseradish peroxidase-conjugated
220 secondary antibodies (1 h) (Supplementary Table 2), for detection with a Chemiluminescent
221 kit (Novex ECL, Invitrogen, WP20005) and a ChemiDoc MP Imaging system (Bio-Rad).
222 Membrane Coomassie (Sigma-Aldrich, 27816) staining was used for loading control rather
223 than 'housekeeping' proteins, as their levels may change under certain conditions (33).
224 Densitometric analyses were performed with the Image J software. In each independent
225 experiment, samples from control (0 µM GSK) and 10 µM GSK- treated zebrafish were run in
226 the same gel.
227
228 **2.9 Bioinformatic analyses**
229 **2.9.1 Comparison of PERK orthologues**
230 Protein sequence data from zebrafish (*Danio rerio,* XP_005156642.2), human (*Homo*
231 *sapiens,* AAI26357.1), mouse (*Mus musculus,* AAH54809.1), and fruit fly (*Drosophila*
232 *melanogaster,* AAF61200.1) were obtained from UniProt (https://www.uniprot.org/,
233 28th February 2025). The amino acid sequences from the total human PERK protein and
234 from its kinase domain were compared with its orthologue proteins from zebrafish,

235 mouse, and fruit fly, using the Protein BLAST tool
236 (https://blast.ncbi.nlm.nih.gov/Blast.cgi). Additionally, we determined the identity of
237 the vital amino acids for GSK2606414 binding to the catalytic site of PERK, by aligning
238 the protein sequence from zebrafish and human.

239 **2.9.2 Zebrafish PERK 3D structure and molecular docking**

240 The predicted three-dimensional protein structures of zebrafish PERK (UniProt:
241 B8JI14) and human PERK (UniProt: Q9NZJ5) were obtained from AlphaFold Protein
242 Structure Database (34, 35). UCSF ChimeraX software was used to visualize, align
243 (Matchmaker tool) and calculate the root-mean-square deviation (RMSD) of the three-
244 dimensional structures of human PERK (PDB: 4g31) and zebrafish PERK (UniProt:
245 B8JI14), and GSK2606414.

246

247 **2.10 Statistical Analyses**

248 Data are shown as mean ± standard error of the mean (SEM) of the *n* specified in figure legends.
249 For experiments with only two groups, comparisons were made with Student's *t*-test. For
250 single-factor (drug concentration) comparisons of multiple groups to their respective control,
251 we used One-Way ANOVA with Dunnett's *post-hoc* test. For two-factor (drug concentration
252 vs. time) analysis, we used Two-Way ANOVA with Sidak's *post-hoc* test. For survival analysis
253 we used the Mantel-Cox (Log-rank) test. $P < 0.05$ was taken as statistically significant. Data
254 analyses were performed with Prism 6.0 (GraphPad).

255 **3. Results**

256

257 **3.1 The PERK-GSK2606414 binding site is conserved in humans and zebrafish**

258 To assess the potential of zebrafish to study PERK function and its pharmacological
259 modulation, we performed bioinformatic comparisons of the amino acid and structural identity
260 of zebrafish and human PERK, including specifically the binding site for the PERK inhibitor
261 GSK2606414. We selected GSK2606414 (hereafter GSK; not to be confused with glycogen
262 synthase kinase) because: it is one of the most used PERK inhibitors (1); it was previously used
263 in zebrafish (15); and the vital amino acids for its binding to PERK are identified (36, 37).

264 The zebrafish PERK homologue presented 59% global amino acid identity with human
265 PERK (Figure 1 A). Using Protein BLAST, we observed that out of the 12 vital amino acids
266 for GSK binding to PERK (36, 37), there is only one difference between human and zebrafish
267 (Figure 1 B). Such difference is a valine in human vs. isoleucine in zebrafish, and both amino
268 acids are hydrophobic. Using molecular visualization with ChimeraX, we observed that the
269 average distance between the 3D structures of zebrafish and human PERK is under 1 Å (Figure
270 1 C, D), indicating high similarity (38).

271 These results predict a high probability of GSK binding and inhibiting zebrafish PERK.
272 To test such prediction, we proceeded with functional assays.

273

274 **3.2 The PERK inhibitor GSK2606414 is bioactive in zebrafish**

275 To evaluate the effects of PERK inhibition, we evaluated the survival and hatching of zebrafish
276 treated with increasing concentrations of GSK over time (Figure 2 A). We observed a time-
277 dependent decrease in survival, with 10 μM GSK being the concentration that induces a
278 significant effect (50%) at 76 hpf (Figure 2 B). For zebrafish that survived GSK, hatching
279 increased time-dependently, without significant differences across GSK concentrations (Figure

280 2 C). Next, we assessed the effect of GSK on the levels of PERK pathway (ISR) biomarkers in
281 the zebrafish at 76 hpf using western blot (Figure 2 D *i*). Treatment with GSK (10 μM, 72h)
282 significantly decreased levels of phosphorylated eIF2α, ATF4, and CHOP (Figure 2 D *ii*-*vi*).
283 Together, GSK effects confirm its bioactivity and are compatible with PERK pathway
284 inhibition as previously reported (15).
285
286 **3.3 PERK inhibition induces morphologic defects in zebrafish**
287 PERK loss-of function elicits skeletal dysplasia in patients (5). To investigate the role of PERK
288 in skeletal development, we exposed zebrafish embryos to the PERK inhibitor from 4 to 76 hpf
289 and monitored their development over time. GSK (10 μM) evoked a significant time-dependent
290 increase in morphological defects (Figure 3 A *i*). The most common defect was a curly-up tail
291 and a few cases of scoliosis (Figures 3 A *ii* - *iv*). Exposure to GSK (10 μM) caused 20 ± 5
292 degrees change in the zebrafish trunk-tail angle at 76 hpf (Figure 3 B) and a significant decrease
293 in body length (Figure 3 C).
294 To ascertain if the morphological defects evoked by GSK originate primarily in
295 developing skeletal or muscular structures, we tested if the defects could be reversed by a
296 muscle relaxant (d-tubocurarine; dTC; antagonist of muscular nicotinic receptors (39);
297 effective in zebrafish (40)). We observed a concentration-dependent decrease in escape
298 responses, with a maximal relaxation effect at 3 mM (Figure 3 D *i,ii*), confirming dTC efficacy
299 as previously described (40). 3 mM dTC did not recover trunk-tail angle in GSK-treated
300 zebrafish (Figure 3 E), indicating that that abnormal skeletal development, rather than muscle
301 contraction, is the main cause of the morphological defects.
302 We measured otolith area (Supplementary Figure 1) and eye/body ratio (Supplementary
303 Figure 2) as negative controls (unrelated with WRS phenotypes) and found no changes upon
304 GSK exposure indicating that GSK effects on zebrafish morphology are selective.

305 These results indicate that upon PERK inhibition, zebrafish presented abnormal skeletal
306 development and growth retardation, indicating that this small vertebrate holds potential to
307 study the role of PERK in skeletal development.
308

309 **3.4 PERK inhibition delays endocrine pancreas development and limits glucose uptake**
310 **in zebrafish**

311 Lack of PERK in WRS patients leads to decreased β-cell mass, impaired insulin production
312 and neonatal diabetes (41, 42). Exocrine pancreas dysfunction was found in only 10.6% of
313 patients (43, 44). Thus, we explored if zebrafish could be useful to study PERK's role in
314 pancreatic development.

315 To ascertain the effects of PERK inhibition in exocrine and endocrine pancreas
316 development, we used two transgenic zebrafish lines expressing GFP in insulin-producing β-
317 cells (Figure 4 A): one line also expressed mCherry in somatostatin-producing δ-cells from the
318 endocrine pancreas – Tg(*ins:GFP, sst:mCherry*); the other line expressed mCherry in elastase-
319 producing exocrine pancreas –Tg(*ins:GFP, ela:mCherry*). We exposed both lines to GSK (10
320 μM) and measured the GFP/mCherry labelled areas as proxies for cell mass.

321 To test if the effects of GSK inhibition were selective for the early embryo
322 development, we used two exposure protocols: the *early exposure protocol* (Figure 4 B *i*)
323 started before the formation of the first Langerhans islet (endocrine pancreas); the *late exposure*
324 *protocol* started after islet formation (Figure 4 B *ii*). Early PERK inhibition (4 hpf) delayed
325 development of the endocrine pancreas, significantly decreasing β and δ cell mass at 28 hpf,
326 which seems to recover overtime (Figure 4 C *i*, D *i*). Late inhibition (76 hpf) failed to alter
327 endocrine cell mass (Figure 4 C *ii*, D *ii*). Regarding the exocrine pancreas mass, *ela:mCherry*
328 fluorescence was only detectable at 148 hpf, and remained unchanged with either early or late

329 GSK exposure protocols (Figure 4 E). These findings support the hypothesis that PERK
330 inhibition delays the early embryonic development of the endocrine pancreas.

331 To test if delayed endocrine development affected glucose homeostasis, we measured
332 the uptake of the fluorescent glucose probe 2-NBDglucose (29) in zebrafish treated with GSK
333 from 4 to 76 hpf (early exposure protocol). 2-NBDglucose uptake was measured in neuromast
334 cells, given their direct exposure to probes in the external media, using Mitotracker Deep Red
335 as a positive control for neuromast staining. Early PERK inhibition significantly decreased the
336 uptake of 2-NBDglucose (Figure 5 A, B), indicating that PERK inhibition, induces a diabetic-
337 like phenotype in zebrafish.

338

339 **3.5 PERK inhibition evokes neuromuscular and cardiac impairments in zebrafish**

340 Beyond diabetes and skeletal dysplasia, patients with loss-of-function mutations in PERK may
341 also present impaired brain development (45), muscle weakness (46) and cardiac alterations
342 (47, 48). We first assessed the role of PERK on zebrafish neuromuscular function by measuring
343 spontaneous tail-coiling and touch-evoked escape responses upon PERK inhibition (49-51).
344 GSK (10 μM) significantly increased tail-coiling events in early development (28 hpf embryos
345 inside the chorion; Figure 6 A) and significantly decreased escape responses in later
346 development (76 hpf larvae; Figure 6 B). To test for altered muscle integrity, we assessed the
347 arrangement of sarcomeres by measuring how well they diffracted polarized light
348 (birefringence assay) (52) (Figure 6 C *i*). Treatment with 10 μM GSK significantly decreased
349 muscle birefringence intensity (Figure 6 C *ii, iii*).

350 Next, we monitored cardiac morphology and function in PERK-inhibited zebrafish, where
351 10 μM GSK induced a time-dependent increase in pericardial oedema (Figure 7 A).
352 Additionally, at 76 hpf, 10 μM GSK induced bradycardia without altering atrio-ventricular
353 coordination in zebrafish (Figure 7 B).

354 These results suggest that PERK-inhibited zebrafish present neuromuscular and cardiac
355 abnormalities in morphology and function, indicating that zebrafish are suitable models to
356 study PERK effects on neuromuscular and cardiac development and function.
357
358
359 **4. Discussion**
360 This study contributes to the understanding of PERK's role in the embryonic development of
361 zebrafish, building on PERK's functions in zebrafish sleep and oxidative stress regulation (15-
362 17). We show that PERK inhibition causes defective skeletal development and diabetic-like
363 phenotypes, cardiac and neuromuscular alterations in zebrafish, mirroring key features of
364 Wolcott-Rallison syndrome patients. These results highlight the potential of zebrafish to study
365 PERK's role in developmental diseases with multisystem involvement such as the WRS.
366 PERK inhibition with GSK2606414 (GSK), one of the most used PERK inhibitors in
367 the scientific literature, decreased ISR activation in animals like mice (53), frogs (54) and flies
368 (15). In the present study, we show that GSK decreases the levels of ISR markers in zebrafish,
369 which suggests that GSK is bioactive and effective in decreasing PERK pathway activity.
370 Additionally, GSK evoked key WRS-associated phenotypes (impaired skeletal development
371 and diabetic-like phenotype), while sparing non-WRS-associated parameters as otolith area
372 and eye/body ratio. Although we cannot exclude GSK off-targeting c-KIT and RIPK kinases
373 (55, 56), zebrafish with genetically inhibited KITa/b and RIPK3 (57, 58) did not show the
374 curly-up tail and other structural alterations reported in our study, suggesting that such
375 alterations are not off-targets effects of GSK in c-KIT and RIPK kinases. Thus, these results
376 are compatible with GSK selectively inhibiting PERK in zebrafish.
377 Loss of PERK function causes growth retardation and skeletal dysplasia in humans (5) and
378 mice, via impairments in collagen secretion, osteoblast differentiation and bone mineralization

379 (9, 59, 60). Here, we show that PERK inhibition in zebrafish causes growth retardation and
380 spinal deformities resistant to muscle relaxation with tubocurarine. Since at the time of the
381 assays (76 hpf) the zebrafish cartilage is starting to ossify (61), our findings indicate that PERK
382 inhibition impairs zebrafish skeletal development.

383 PERK controls pancreatic β-cell development and insulin production (62). Loss of PERK
384 function in humans and mice causes decreased pancreatic mass and neonatal diabetes, by
385 impairing β-cell proliferation and proinsulin maturation in the endoplasmic reticulum (63-66).
386 Here we show that PERK inhibition during early zebrafish development delays endocrine
387 pancreas formation, resulting in a decreased β-cell mass, which gradually recovers overtime.
388 To assesses whether glucose homeostasis is impaired in PERK-inhibited zebrafish we used the
389 fluorescence glucose uptake probe 2-NBDglucose. We found reduced 2-NBDglucose uptake,
390 which indicates that glucose homeostasis remains partly compromised despite the ongoing β-
391 cell mass recovery. Such recovery in the presence of GSK suggests that zebrafish can
392 regenerate pancreatic tissue (67, 68) by PERK-independent mechanisms. The identification of
393 such PERK-independent mechanisms in zebrafish may assist the development of novel
394 therapies for β-cell regeneration for human diabetes (69).

395 In contrast to the delayed development of the zebrafish endocrine pancreas, we found no
396 effect of PERK-inhibition upon the mass of the exocrine pancreas. While different mechanisms
397 regulate development of the endocrine and exocrine pancreas (43, 65), we cannot exclude that
398 extended exposure of zebrafish to the PERK inhibitor may alter the mass of the exocrine
399 pancreas. Future studies using selective PERK knockout in zebrafish pancreatic cell sub-types
400 may contribute to understand differential pancreatic vulnerability.

401 Beyond pancreatic dysfunction, PERK inhibition in humans and mice impairs neuronal
402 and muscular functions (5, 6, 11, 70, 71). Here we show that PERK inhibition in zebrafish
403 increases spontaneous tail movements early in development, which arise in a spinal central

404 pattern generator that provides rhythmic depolarizations (49, 51), and decreases touch-evoked
405 escape responses later in development, which arise in sensory neurons (50, 51). We also show
406 that PERK-inhibited zebrafish display altered muscular integrity, likely contributing to
407 decreased escape responses. Thus, as with mammals, the mechanisms underlying motor
408 impairment in PERK-inhibited zebrafish combine dysfunctions in neurons and muscle.

409 Patients and mice with PERK loss of function often display cardiac malformations (10,
410 47, 48). Here we show that PERK-inhibited zebrafish display cardiac abnormalities, such as
411 oedema and bradycardia. The transparency and small size of young zebrafish is amenable to
412 the detection of cardiac abnormalities that would be fatal in larger animals due to insufficient
413 oxygen diffusion (72). Moreover, zebrafish may assist discovery of heart regeneration
414 mechanisms (73). Thus, future studies with a more detailed structural and functional
415 characterization of the cardiac abnormalities in PERK-inhibited or deleted zebrafish, may
416 provide valuable insights into disease mechanisms and potential therapeutics.

417

418 **5. Conclusions**

419 This study highlights the potential of the small vertebrate zebrafish as a model for
420 developmental diseases, namely those caused by PERK inhibition like the WRS. We show that
421 pharmacological inhibition of PERK with GSK2606414 mimicked WRS pathophysiology by
422 inducing defective growth and skeletal development, and diabetic-like phenotypes such as
423 delayed development of the endocrine pancreas and altered glucose homeostasis. PERK
424 inhibition also impaired neuromuscular and cardiac development, while sparing non-WRS
425 associated parameters like otolith area and eye/body ratio. Future studies using CRISPR/Cas9
426 technology can be used to generate zebrafish models with conditional/selective expression of
427 human PERK with WRS-driving mutations (74). Also, future research on the mechanisms
428 governing PERK-independent pancreatic regeneration in zebrafish may uncover potential

429 therapeutic targets for diabetes. Further, the scalability of zebrafish models holds great
430 potential to enhance the efficiency of drug screening against PERK-associated developmental
431 diseases.

Declarations

Authorship contribution

Conceptualization – LA, BRP, JMAO**; Methodology –** LA, NASO, JB, BRP, JMAO; **Investigation –** LA, LPL, NASO, RFOS, BS; **Validation** – LA, LPL, NASO, RFOS, BS; **Data Curation** – LA; **Formal Analysis** – LA, LPL, NASO, RFOS; **Visualization** – LA, LPS, NASO; **Writing – original draft** – LA; **Writing – review and editing** – LA, LPL, NASO, JB, BRP, JMAO; **Resources** – JB, JMAO; **Funding acquisition** – JB, JMAO; **Project administration** – JMAO; **Supervision –** BRP, JMAO.

Funding

JMAO's laboratory - FCT – Fundação para a Ciência e a Tecnologia, Portugal – (UIDB/04378/2020; UIDP/04378/2020; LA/P/0140/2020). LMA - FCT PhD fellowship - SFRH/BD/138451/2018. BRP - FCT funding program DL57/2016 - Norma transitória (DL57/2016/CP1346/CT0016). JB's laboratory - FCT project PTDC/BIA-MOL/3834/2021. JB's FCT contract CEECIND/03482/2018.

Conflict of interest statement

No financial or non-financial interests to disclose.

Data availability statement

The datasets generated during and/or analysed during the current study are available from the corresponding author upon reasonable request.

457 **Figure legends**

458

459 **Figure 1.** Bioinformatic analyses of PERK identity and GSK2606414-binding in human vs.
460 zebrafish. (**A**) Percentage of identity between human, fruit fly (*Drosophila melanogaster*),
461 zebrafish (*Danio rerio*), and mouse (*Mus musculus*) PERK (total and kinase domain); Protein
462 BLAST. (**B**) Comparing vital GSK2606414 (GSK)-binding amino acids in the catalytic domain
463 of human and zebrafish PERK. Valine 651 in human (yellow) is substituted by the also
464 hydrophobic Isoleucine 671 (red) in zebrafish; Protein BLAST. (**C**) Predicted GSK (purple, #)
465 binding to human (light blue) and zebrafish (dark blue) PERK; ChimeraX. (**D**) Root Mean
466 Square Deviation (RMSD) comparing human and zebrafish PERK tertiary structures and
467 respective reference values; ChimeraX.

468

469 **Figure 2.** GSK2606414 effects on zebrafish survival, hatching, and PERK pathway
470 biomarkers. (**A**) Experimental timeline. (**B**) Zebrafish survival when exposed to GSK2606414
471 (GSK; 0-10 μM) over time (4-76 hours post-fertilization; hpf); n = 50-234 zebrafish, 5
472 independent breedings, Mantel-Cox test for survival, $^{*}P < 0.05$ vs. 0 μM GSK (control). (**C**)
473 Hatching of zebrafish treated with GSK; n= 50-234 zebrafish, 5 breedings, Two-Way ANOVA,
474 time effect: $^{\#}P < 0.05$. (**D**) Western blot of live 76 hpf zebrafish: *i*) Schematic representation
475 of the PERK pathway biomarkers; *ii-vi*) Representative blots and quantifications; n = 4
476 independent experiments (pool of 24-27 larvae per condition and per experiment); *t*-test: $^{*}P <$
477 0.05.

478

479 **Figure 3.** GSK2606414 impaired skeletal development in zebrafish. (**A**) (*i*) Morphological
480 defects following GSK2606414 (GSK) (0-10 μM) treatment overtime; $^{*}P < 0.05$, 10 vs. 0 μM
481 GSK; $^{\#}P<0.05$, effect of time for 10 μM GSK, Two-Way ANOVA with Sidak *post-hoc*; n =

482 50-234 zebrafish; 5 independent experiments. (*ii-v*) Proportion of curly-up tail and scoliosis at
483 76 hpf, and representative images. (**B, C**) Measurements (blue lines) and quantifications of
484 trunk-tail angle and body length at 76 hpf; *$P < 0.05$ vs 0 μM GSK, One-Way ANOVA with
485 Dunnett's *post-hoc*; $n = 15$ zebrafish, 3 independent experiments. (**D**) Effect of muscle relaxant
486 d-tubocurarine (dTC, 0.03–3 mM) on escape responses after head or tail touch at 76 hpf; Grey
487 bands are mean ± SEM for control zebrafish; *$P < 0.05$ vs 0 mM dTC, One-Way ANOVA with
488 Dunnett's *post-hoc,* $n = 15$ zebrafish, 3 independent experiments. (**E**) (*i-iv*) Representative
489 images of zebrafish for the indicated-treatments. (*v*) Quantification of zebrafish with
490 morphological defects at 76 hpf for the indicated treatments. *$P < 0.05$ vs control, One-Way
491 ANOVA with Sidak's *post-hoc*, $n = 15$ zebrafish; 3 independent breedings. Blue arrows: curly-
492 up tail.
493
494 **Figure 4.** Pancreatic development in transgenic zebrafish. **(A)** Representative images of normal
495 pancreas development in Tg(*ins:GFP, sst:mCherry*) and Tg(*ins:GFP, ela:mCherry*) zebrafish.
496 (**B)** early (*i*) and late (*ii*) GSK2606414 (GSK)-exposure protocols. (**C-E**) Area measurements
497 for *ins:GFP* (green, insulin-producing *β*-cells), *sst:mCherry* (red, somatostatin-producing *δ*-
498 cells), and *ela:mCherry* (red, elastase-producing exocrine cells), in zebrafish exposed to 10 μM
499 GSK since 4 hpf (*i*, early exposure) or since 76 hpf (*ii*, late exposure). *$P < 0.05$, *t*-test, $n = 4$-
500 33 larvae. Representative images of GFP and mCherry are shown below respective bars. Scale
501 bars indicate 200 μm.
502
503 **Figure 5.** GSK2606414 effects on 2-NBDglucose uptake in zebrafish. (**A**) Representative
504 brightfield and fluorescence images of zebrafish at 76 hpf, following treatment with (*i*) 0 μM
505 (control) or (*ii*) 10 μM GSK2606414 since 4 hpf. Images show functional labelling at 76 hpf
506 with the fluorescent glucose analogue 2-NBDglucose (2-NBDG) for neuromasts that uptake

507 glucose, and with MitoTracker Deep Red that labels mitochondria in neuromasts as positive
508 control. In the "Merge" images, yellow circles highlight neuromasts with both 2-NBDglucose
509 and MitoTracker, while red circles highlight those containing MitoTracker only. Below, 2x
510 amplified images show neuromasts from the zebrafish lateral line, with arrows indicating
511 neuromasts on the side proximal to the microscope objective (the paired neuromasts on the
512 opposite side are unmarked). (**B**) Quantification of neuromasts labelled with 2-NBDglucose.
513 *$P < 0.05$, t-test, n = 9-12 zebrafish per condition.
514
515 **Figure 6.** GSK2606414 effects on neuromotor responses and muscle integrity. (**A**) (*i*)
516 Representative tail coiling time-lapse: white line highlights notochord movement. (*ii*)
517 Quantification of tail coiling in 28 hpf zebrafish treated with GSK2606414 since 4 hpf; n = 23-
518 26 zebrafish. (**B**) Quantification of escape responses after head (*i*) or tail (*ii*) touches at 76 hpf;
519 n = 13-114 zebrafish. (**C**) (*i*) Schematic representation of the birefringence assay for muscle
520 integrity; (*ii*) Representative images of muscle birefringence at 76 hpf. (*iii*) Quantification of
521 birefringence intensity; n = 15 zebrafish. (**A-C**) Grey bands are mean ± SEM for 0 μM GSK
522 (control); *$P < 0.05$ vs. (control), One-Way ANOVA with Dunnett's *post-hoc*.
523
524 **Figure 7.** GSK2606414-induced morphological and functional cardiac defects. (**A**) (*i*)
525 Quantification of live zebrafish with pericardial oedema at the indicated hpf and GSK
526 concentrations. *$P < 0.05$, 10 vs. 0 μM GSK (control); Two-Way ANOVA with Sidak *post-*
527 *hoc* n= 50-234 zebrafish; 5 independent experiments. (*ii,iii*) Representative images of zebrafish
528 treated with GSK vs. control; blue arrow: pericardial oedema. (**B**) (*i*) Heartbeats per minute
529 (bpm) of 76 hpf zebrafish exposed to increasing GSK concentrations since 4 hpf; Grey band is
530 mean ± SEM for control; *$P < 0.05$ vs control, One-Way ANOVA with Dunnett's *post-hoc*, n

531 = 13-116 zebrafish; (*ii*) Representative images of the heart and plots of atrio-ventricular
532 coordination in control and 10 μM GSK-treated zebrafish (a: atrium – red; v: ventricle – blue).
533

534 **References**

535

536 1. Almeida LM, Pinho BR, Duchen MR, Oliveira JMA. The PERKs of mitochondria
537 protection during stress: insights for PERK modulation in neurodegenerative and metabolic
538 diseases. Biol Rev Camb Philos Soc. 2022.

539 2. Peshkin L, Wuhr M, Pearl E, Haas W, Freeman RM, Jr., Gerhart JC, et al. On the
540 Relationship of Protein and mRNA Dynamics in Vertebrate Embryonic Development. Dev
541 Cell. 2015;35(3):383-94.

542 3. Wang P, Li J, Tao J, Sha B. The luminal domain of the ER stress sensor protein PERK
543 binds misfolded proteins and thereby triggers PERK oligomerization. J Biol Chem.
544 2018;293(11):4110-21.

545 4. Senee V, Vattem KM, Delepine M, Rainbow LA, Haton C, Lecoq A, et al. Wolcott-
546 Rallison Syndrome: clinical, genetic, and functional study of EIF2AK3 mutations and
547 suggestion of genetic heterogeneity. Diabetes. 2004;53(7):1876-83.

548 5. Julier C, Nicolino M. Wolcott-Rallison syndrome. Orphanet J Rare Dis. 2010;5:29.

549 6. Bruch J, Kurz C, Vasiljevic A, Nicolino M, Arzberger T, Hoglinger GU. Early
550 Neurodegeneration in the Brain of a Child Without Functional PKR-like Endoplasmic
551 Reticulum Kinase. J Neuropathol Exp Neurol. 2015;74(8):850-7.

552 7. Tzakis AG, Nunnelley MJ, Tekin A, Buccini LD, Garcia J, Uchida K, et al. Liver,
553 pancreas and kidney transplantation for the treatment of Wolcott-Rallison syndrome. Am J
554 Transplant. 2015;15(2):565-7.

555 8. Harding HP, Zeng H, Zhang Y, Jungries R, Chung P, Plesken H, et al. Diabetes mellitus
556 and exocrine pancreatic dysfunction in perk-/- mice reveals a role for translational control in
557 secretory cell survival. Mol Cell. 2001;7(6):1153-63.

558 9. Zhang P, McGrath B, Li S, Frank A, Zambito F, Reinert J, et al. The PERK eukaryotic
559 initiation factor 2 alpha kinase is required for the development of the skeletal system, postnatal
560 growth, and the function and viability of the pancreas. Mol Cell Biol. 2002;22(11):3864-74.
561 10. Shimizu T, Maruyama K, Kawamura T, Urade Y, Wada Y. PERK participates in
562 cardiac valve development via fatty acid oxidation and endocardial-mesenchymal
563 transformation. Sci Rep. 2020;10(1):20094.
564 11. Gallot YS, Bohnert KR, Straughn AR, Xiong G, Hindi SM, Kumar A. PERK regulates
565 skeletal muscle mass and contractile function in adult mice. FASEB J. 2019;33(2):1946-62.
566 12. Trinh MA, Kaphzan H, Wek RC, Pierre P, Cavener DR, Klann E. Brain-specific
567 disruption of the eIF2alpha kinase PERK decreases ATF4 expression and impairs behavioral
568 flexibility. Cell Rep. 2012;1(6):676-88.
569 13. Teame T, Zhang Z, Ran C, Zhang H, Yang Y, Ding Q, et al. The use of zebrafish (Danio
570 rerio) as biomedical models. Anim Front. 2019;9(3):68-77.
571 14. Choi TY, Choi TI, Lee YR, Choe SK, Kim CH. Zebrafish as an animal model for
572 biomedical research. Exp Mol Med. 2021;53(3):310-7.
573 15. Ly S, Lee DA, Strus E, Prober DA, Naidoo N. Evolutionarily Conserved Regulation of
574 Sleep by the Protein Translational Regulator PERK. Curr Biol. 2020;30(9):1639-48 e3.
575 16. Jin B, Xie L, Zhan D, Zhou L, Feng Z, He J, et al. Nrf2 dictates the neuronal survival
576 and differentiation of embryonic zebrafish harboring compromised alanyl-tRNA synthetase.
577 Development. 2022;149(17).
578 17. Mukaigasa K, Tsujita T, Nguyen VT, Li L, Yagi H, Fuse Y, et al. Nrf2 activation
579 attenuates genetic endoplasmic reticulum stress induced by a mutation in the
580 phosphomannomutase 2 gene in zebrafish. Proc Natl Acad Sci U S A. 2018;115(11):2758-63.

581 18. Stockwell SR, Platt G, Barrie SE, Zoumpoulidou G, Te Poele RH, Aherne GW, et al.
582 Mechanism-based screen for G1/S checkpoint activators identifies a selective activator of
583 EIF2AK3/PERK signalling. PLoS One. 2012;7(1):e28568.
584 19. Oliveira NAS, Pinho BR, Pinto J, Guedes de Pinho P, Oliveira JMA. Edaravone
585 counteracts redox and metabolic disruptions in an emerging zebrafish model of sporadic ALS.
586 Free Radic Biol Med. 2024;217:126-40.
587 20. Hoyberghs J, Bars C, Ayuso M, Van Ginneken C, Foubert K, Van Cruchten S. DMSO
588 Concentrations up to 1% are Safe to be Used in the Zebrafish Embryo Developmental Toxicity
589 Assay. Front Toxicol. 2021;3:804033.
590 21. Silva RFO, Pinho BR, Santos MM, Oliveira JMA. Disruptions of circadian rhythms,
591 sleep, and stress responses in zebrafish: New infrared-based activity monitoring assays for
592 toxicity assessment. Chemosphere. 2022;305:135449.
593 22. Pinho BR, Reis SD, Hartley RC, Murphy MP, Oliveira JMA. Mitochondrial superoxide
594 generation induces a parkinsonian phenotype in zebrafish and huntingtin aggregation in human
595 cells. Free Radic Biol Med. 2019;130:318-27.
596 23. OECD. Test No. 236: Fish Embryo Acute Toxicity (FET) Test. 2013.
597 24. Kimmel CB, Ballard WW, Kimmel SR, Ullmann B, Schilling TF. Stages of embryonic
598 development of the zebrafish. Dev Dyn. 1995;203(3):253-310.
599 25. Martinez R, Navarro-Martin L, Luccarelli C, Codina AE, Raldua D, Barata C, et al.
600 Unravelling the mechanisms of PFOS toxicity by combining morphological and transcriptomic
601 analyses in zebrafish embryos. Sci Total Environ. 2019;674:462-71.
602 26. Pinho BR, Santos MM, Fonseca-Silva A, Valentao P, Andrade PB, Oliveira JM. How
603 mitochondrial dysfunction affects zebrafish development and cardiovascular function: an in
604 vivo model for testing mitochondria-targeted drugs. Br J Pharmacol. 2013;169(5):1072-90.

605 27. Oliveira NAS, Pinho BR, Oliveira JMA. Swimming against ALS: How to model
606 disease in zebrafish for pathophysiological and behavioral studies. Neurosci Biobehav Rev.
607 2023;148:105138.
608 28. Pinho BR, Reis SD, Guedes-Dias P, Leitao-Rocha A, Quintas C, Valentao P, et al.
609 Pharmacological modulation of HDAC1 and HDAC6 in vivo in a zebrafish model: Therapeutic
610 implications for Parkinson's disease. Pharmacol Res. 2016;103:328-39.
611 29. Lee J, Jung DW, Kim WH, Um JI, Yim SH, Oh WK, et al. Development of a highly
612 visual, simple, and rapid test for the discovery of novel insulin mimetics in living vertebrates.
613 ACS Chem Biol. 2013;8(8):1803-14.
614 30. Wang L, Kong H, Jin M, Li X, Stoika R, Lin H, et al. Synthesis of disaccharide modified
615 berberine derivatives and their anti-diabetic investigation in zebrafish using a fluorescence-
616 based technology. Org Biomol Chem. 2020;18(18):3563-74.
617 31. Stengel D, Zindler F, Braunbeck T. An optimized method to assess ototoxic effects in
618 the lateral line of zebrafish (Danio rerio) embryos. Comp Biochem Physiol C Toxicol
619 Pharmacol. 2017;193:18-29.
620 32. Tiso N, Moro E, Argenton F. Zebrafish pancreas development. Mol Cell Endocrinol.
621 2009;312(1-2):24-30.
622 33. Li R, Shen Y. An old method facing a new challenge: re-visiting housekeeping proteins
623 as internal reference control for neuroscience research. Life Sci. 2013;92(13):747-51.
624 34. Jumper J, Evans R, Pritzel A, Green T, Figurnov M, Ronneberger O, et al. Highly
625 accurate protein structure prediction with AlphaFold. Nature. 2021;596(7873):583-9.
626 35. Varadi M, Anyango S, Deshpande M, Nair S, Natassia C, Yordanova G, et al.
627 AlphaFold Protein Structure Database: massively expanding the structural coverage of protein-
628 sequence space with high-accuracy models. Nucleic Acids Res. 2022;50(D1):D439-D44.

629 36. Axten JM, Medina JR, Feng Y, Shu A, Romeril SP, Grant SW, et al. Discovery of 7-
630 methyl-5-(1-{[3-(trifluoromethyl)phenyl]acetyl}-2,3-dihydro-1H-indol-5-yl)-7H-p
631 yrrolo[2,3-d]pyrimidin-4-amine (GSK2606414), a potent and selective first-in-class inhibitor
632 of protein kinase R (PKR)-like endoplasmic reticulum kinase (PERK). J Med Chem.
633 2012;55(16):7193-207.
634 37. Chintha C, Carlesso A, Gorman AM, Samali A, Eriksson LA. Molecular modeling
635 provides a structural basis for PERK inhibitor selectivity towards RIPK1. RSC Adv.
636 2019;10(1):367-75.
637 38. Carugo O, Pongor S. A normalized root-mean-square distance for comparing protein
638 three-dimensional structures. Protein Sci. 2001;10(7):1470-3.
639 39. Rahman MM, Basta T, Teng J, Lee M, Worrell BT, Stowell MHB, et al. Structural
640 mechanism of muscle nicotinic receptor desensitization and block by curare. Nat Struct Mol
641 Biol. 2022;29(4):386-94.
642 40. Guzman L, Besa G, Linares D, González L, Pont C, Bartolini M, et al. Evaluation of
643 the effects of acetylcholinesterase inhibitors in the zebrafish touch-evoked response:
644 quantitative vs. qualitative assessment. Environ Sci Eur. 2020;32:12.
645 41. Sumegi A, Hendrik Z, Gall T, Felszeghy E, Szakszon K, Antal-Szalmas P, et al. A
646 novel splice site indel alteration in the EIF2AK3 gene is responsible for the first cases of
647 Wolcott-Rallison syndrome in Hungary. BMC Med Genet. 2020;21(1):61.
648 42. Rubio-Cabezas O, Patch AM, Minton JA, Flanagan SE, Edghill EL, Hussain K, et al.
649 Wolcott-Rallison syndrome is the most common genetic cause of permanent neonatal diabetes
650 in consanguineous families. J Clin Endocrinol Metab. 2009;94(11):4162-70.
651 43. Iida K, Li Y, McGrath BC, Frank A, Cavener DR. PERK eIF2 alpha kinase is required
652 to regulate the viability of the exocrine pancreas in mice. BMC Cell Biol. 2007;8:38.

653 44. Aldrian D, Bochdansky C, Kavallar AM, Mayerhofer C, Deeb A, Habeb A, et al.
654 Natural history of Wolcott-Rallison syndrome: A systematic review and follow-up study. Liver
655 Int. 2024;44(3):811-22.
656 45. de Wit MC, de Coo IF, Julier C, Delepine M, Lequin MH, van de Laar I, et al.
657 Microcephaly and simplified gyral pattern of the brain associated with early onset insulin-
658 dependent diabetes mellitus. Neurogenetics. 2006;7(4):259-63.
659 46. Abdelmeguid Y, Mowafy EW, Marzouk I, Franco E, ElSayed S. Clinical and molecular
660 characteristics of infantile-onset diabetes mellitus in Egypt. Ann Pediatr Endocrinol Metab.
661 2022;27(3):214-22.
662 47. Thornton CM, Carson DJ, Stewart FJ. Autopsy findings in the Wolcott-Rallison
663 syndrome. Pediatr Pathol Lab Med. 1997;17(3):487-96.
664 48. Bejiqi R, Retkoceri R, Zeka N, Bejiqi R, Bejic S. An Infant With Neonatal Diabetes
665 and Double Outlet Right Ventricle - Wolcott- Rallison syndrome. Med Arch. 2018;72(4):289-
666 91.
667 49. Zindler F, Beedgen F, Brandt D, Steiner M, Stengel D, Baumann L, et al. Analysis of
668 tail coiling activity of zebrafish (Danio rerio) embryos allows for the differentiation of
669 neurotoxicants with different modes of action. Ecotoxicol Environ Saf. 2019;186:109754.
670 50. Roberts AC, Chornak J, Alzagatiti JB, Ly DT, Bill BR, Trinkeller J, et al. Rapid
671 habituation of a touch-induced escape response in Zebrafish (Danio rerio) Larvae. PLoS One.
672 2019;14(4):e0214374.
673 51. von Wyl M, Konemann S, Vom Berg C. Different developmental insecticide exposure
674 windows trigger distinct locomotor phenotypes in the early life stages of zebrafish.
675 Chemosphere. 2023;317:137874.
676 52. Berger J, Sztal T, Currie PD. Quantification of birefringence readily measures the level
677 of muscle damage in zebrafish. Biochem Biophys Res Commun. 2012;423(4):785-8.

678 53. Moreno JA, Halliday M, Molloy C, Radford H, Verity N, Axten JM, et al. Oral
679 treatment targeting the unfolded protein response prevents neurodegeneration and clinical
680 disease in prion-infected mice. Sci Transl Med. 2013;5(206):206ra138.
681 54. Cagnetta R, Wong HH, Frese CK, Mallucci GR, Krijgsveld J, Holt CE. Noncanonical
682 Modulation of the eIF2 Pathway Controls an Increase in Local Translation during Neural
683 Wiring. Mol Cell. 2019;73(3):474-89 e5.
684 55. Rojas-Rivera D, Delvaeye T, Roelandt R, Nerinckx W, Augustyns K, Vandenabeele P,
685 et al. When PERK inhibitors turn out to be new potent RIPK1 inhibitors: critical issues on the
686 specificity and use of GSK2606414 and GSK2656157. Cell Death Differ. 2017;24(6):1100-10.
687 56. Mahameed M, Wilhelm T, Darawshi O, Obiedat A, Tommy WS, Chintha C, et al. The
688 unfolded protein response modulators GSK2606414 and KIRA6 are potent KIT inhibitors. Cell
689 Death Dis. 2019;10(4):300.
690 57. Wen W, Chen J, Zhou Y, Li G, Zhang Y. Loss of Ripk3 attenuated neutrophil
691 accumulation in a lipopolysaccharide-induced zebrafish inflammatory model. Cell Death
692 Discov. 2022;8(1):88.
693 58. Hultman KA, Bahary N, Zon LI, Johnson SL. Gene Duplication of the zebrafish kit
694 ligand and partitioning of melanocyte development functions to kit ligand a. PLoS Genet.
695 2007;3(1):e17.
696 59. Li Y, Iida K, O'Neil J, Zhang P, Li S, Frank A, et al. PERK eIF2alpha kinase regulates
697 neonatal growth by controlling the expression of circulating insulin-like growth factor-I
698 derived from the liver. Endocrinology. 2003;144(8):3505-13.
699 60. Wei J, Sheng X, Feng D, McGrath B, Cavener DR. PERK is essential for neonatal
700 skeletal development to regulate osteoblast proliferation and differentiation. J Cell Physiol.
701 2008;217(3):693-707.

702 61. Tonelli F, Bek JW, Besio R, De Clercq A, Leoni L, Salmon P, et al. Zebrafish: A
703 Resourceful Vertebrate Model to Investigate Skeletal Disorders. Front Endocrinol (Lausanne).
704 2020;11:489.
705 62. Cavener DR, Gupta S, McGrath BC. PERK in beta cell biology and insulin biogenesis.
706 Trends Endocrinol Metab. 2010;21(12):714-21.
707 63. Welters A, Meissner T, Konrad K, Freiberg C, Warncke K, Judmaier S, et al. Diabetes
708 management in Wolcott-Rallison syndrome: analysis from the German/Austrian DPV
709 database. Orphanet J Rare Dis. 2020;15(1):100.
710 64. Feng D, Wei J, Gupta S, McGrath BC, Cavener DR. Acute ablation of PERK results in
711 ER dysfunctions followed by reduced insulin secretion and cell proliferation. BMC Cell Biol.
712 2009;10:61.
713 65. Zhang W, Feng D, Li Y, Iida K, McGrath B, Cavener DR. PERK EIF2AK3 control of
714 pancreatic beta cell differentiation and proliferation is required for postnatal glucose
715 homeostasis. Cell Metab. 2006;4(6):491-7.
716 66. Sowers CR, Wang R, Bourne RA, McGrath BC, Hu J, Bevilacqua SC, et al. The protein
717 kinase PERK/EIF2AK3 regulates proinsulin processing not via protein synthesis but by
718 controlling endoplasmic reticulum chaperones. J Biol Chem. 2018;293(14):5134-49.
719 67. Moss JB, Koustubhan P, Greenman M, Parsons MJ, Walter I, Moss LG. Regeneration
720 of the pancreas in adult zebrafish. Diabetes. 2009;58(8):1844-51.
721 68. Pisharath H, Rhee JM, Swanson MA, Leach SD, Parsons MJ. Targeted ablation of beta
722 cells in the embryonic zebrafish pancreas using E. coli nitroreductase. Mech Dev.
723 2007;124(3):218-29.
724 69. Karampelias C, Liu KC, Tengholm A, Andersson O. Mechanistic insights and
725 approaches for beta cell regeneration. Nat Chem Biol. 2025.

726 70. Asl SN, Vakili R, Vakili S, Soheilipour F, Hashemipour M, Ghahramani S, et al.
727 Wolcott-Rallison syndrome in Iran: a common cause of neonatal diabetes. J Pediatr Endocrinol
728 Metab. 2019;32(6):607-13.
729 71. Longo F, Mancini M, Ibraheem PL, Aryal S, Mesini C, Patel JC, et al. Cell-type-
730 specific disruption of PERK-eIF2alpha signaling in dopaminergic neurons alters motor and
731 cognitive function. Mol Psychiatry. 2021;26(11):6427-50.
732 72. Bournele D, Beis D. Zebrafish models of cardiovascular disease. Heart Fail Rev.
733 2016;21(6):803-13.
734 73. Ross Stewart KM, Walker SL, Baker AH, Riley PR, Brittan M. Hooked on heart
735 regeneration: the zebrafish guide to recovery. Cardiovasc Res. 2022;118(7):1667-79.
736 74. Cornet C, Di Donato V, Terriente J. Combining Zebrafish and CRISPR/Cas9: Toward
737 a More Efficient Drug Discovery Pipeline. Front Pharmacol. 2018;9:703.
738

Figures

A Global amino acid comparison

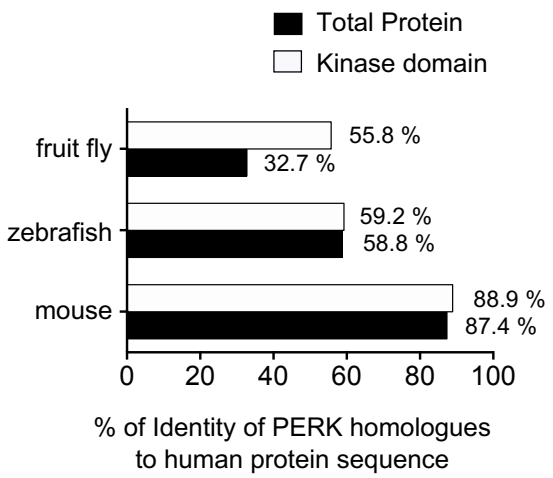

B Comparison of vital* amino acids in kinase domain

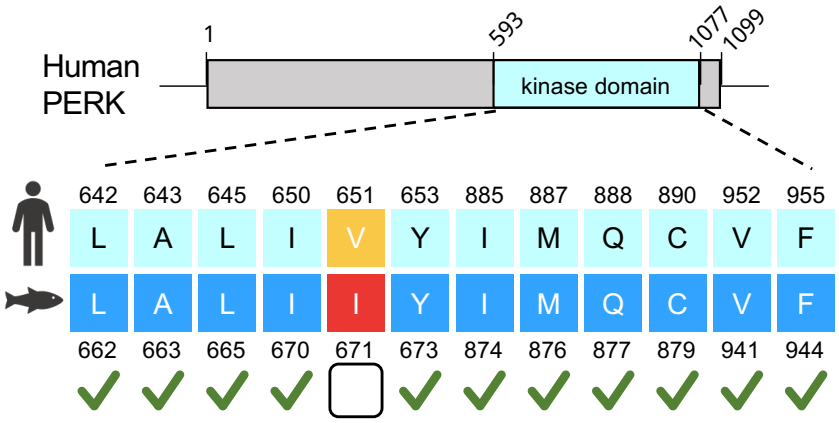

* 12 vital amino acids for GSK2606414 binding

valine (V) and isoleucine (I) are both hydrophobic

C Molecular visualization of GSK binding to PERK

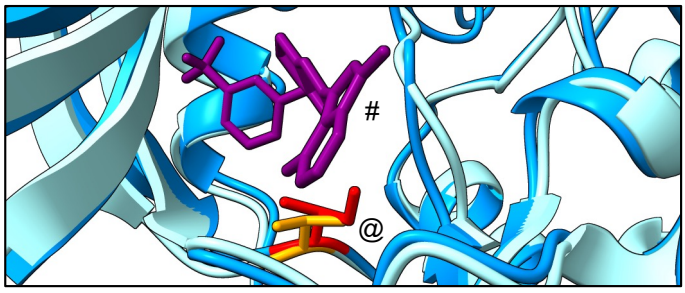

- human PERK
- zebrafish PERK
- @, valine 651 (human)
- @, isoleucine 671 (zebrafish)
- #, GSK2606414 (GSK)

D Structural similarity of human vs. zebrafish PERK

Root Mean Square Deviation		
Total protein	0.868 Å	**High similarity** (0-1 Å)
Catalytic domain	0.371 Å	**High similarity** (0-1 Å)

Figure 1

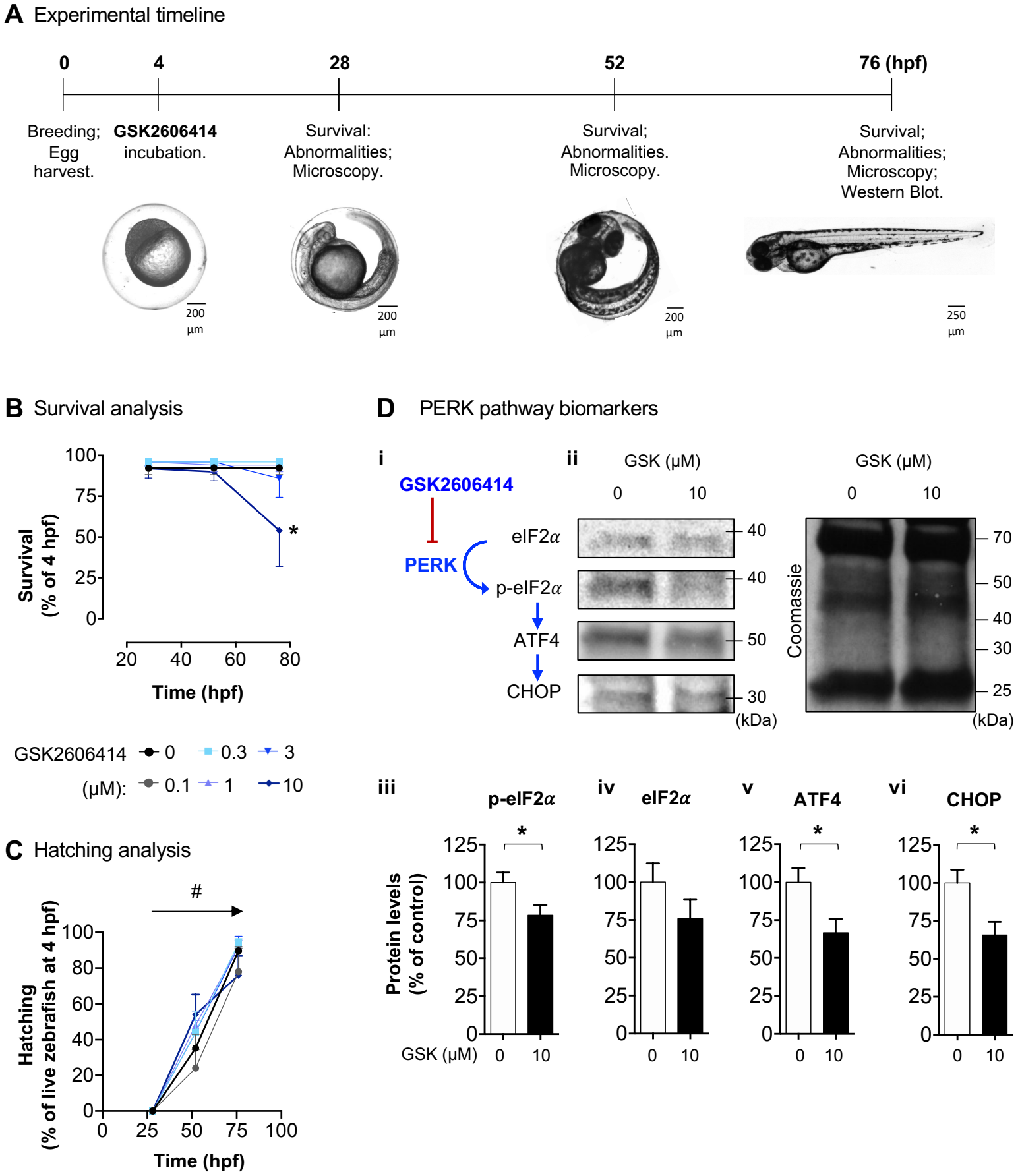
A Experimental timeline
0
4
28
52
76 (hpf)
Breeding; Egg harvest.
GSK2606414 incubation.
Survival: Abnormalities; Microscopy.
Survival; Abnormalities. Microscopy.
Survival; Abnormalities; Microscopy; Western Blot.
200 µm
200 µm
200 µm
250 µm
B Survival analysis
Survival (% of 4 hpf)
Time (hpf)
GSK2606414 (µM): 0 0.3 3 0.1 1 10
C Hatching analysis
Hatching (% of live zebrafish at 4 hpf)
Time (hpf)
D PERK pathway biomarkers
i
GSK2606414
PERK
eIF2α
p-eIF2α
ATF4
CHOP
ii
GSK (µM)
Coomassie
(kDa)
iii p-eIF2α
iv eIF2α
v ATF4
vi CHOP
Protein levels (% of control)
GSK (µM)

Figure 2

A Morphological defects

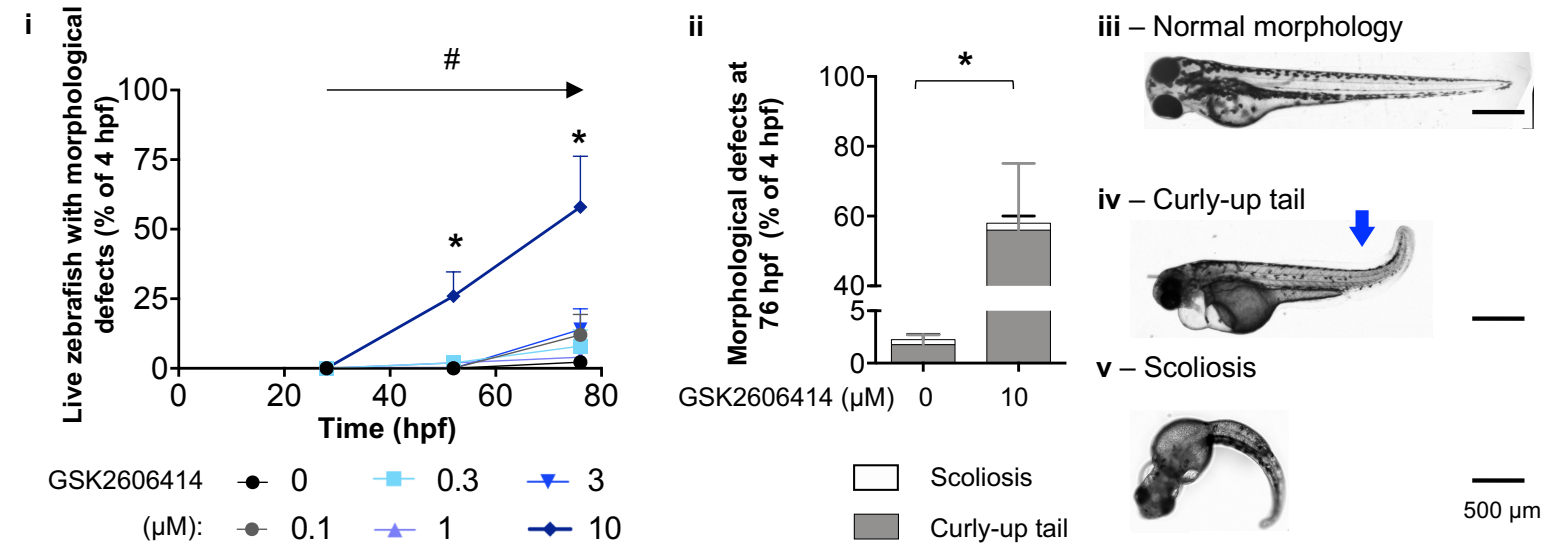

B Trunk-tail angle

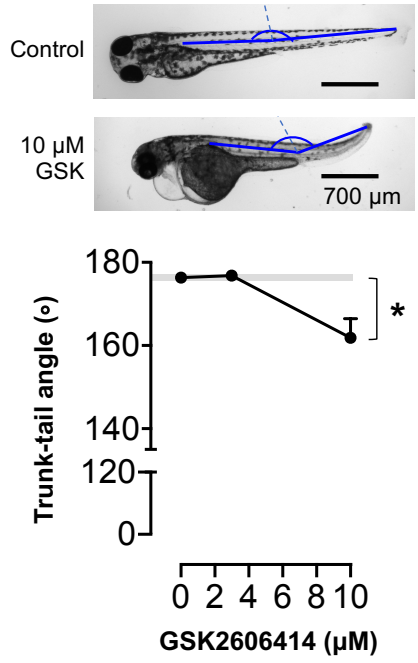

C Body length

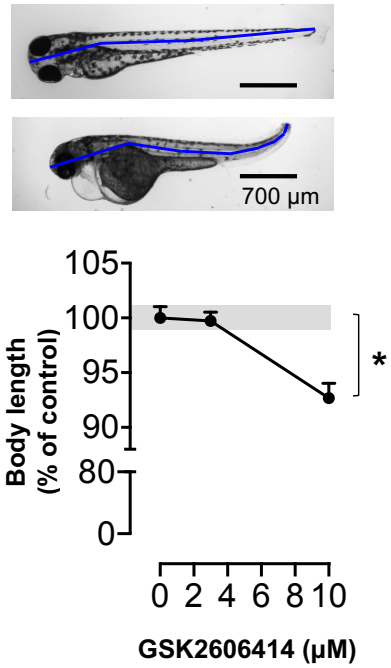

D **Positive control for tubocurarine (dTC)**

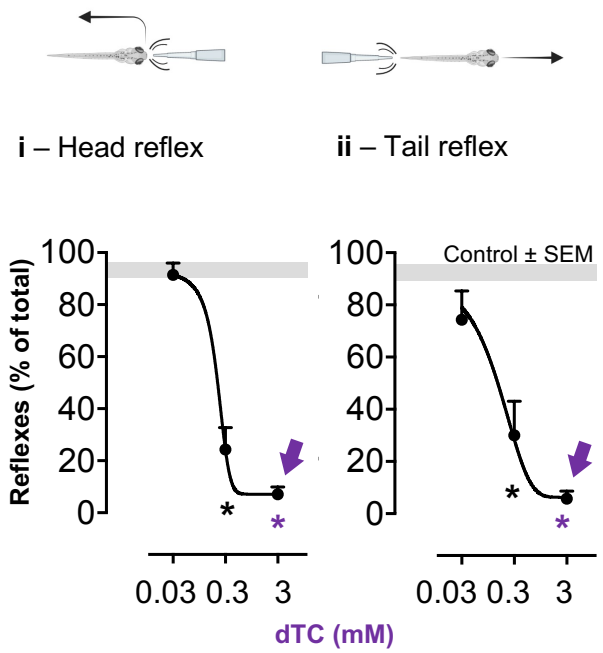

E **The muscle relaxant tubocurarine (dTC) does not rescue the curly-up tail evoked by GSK2606414**

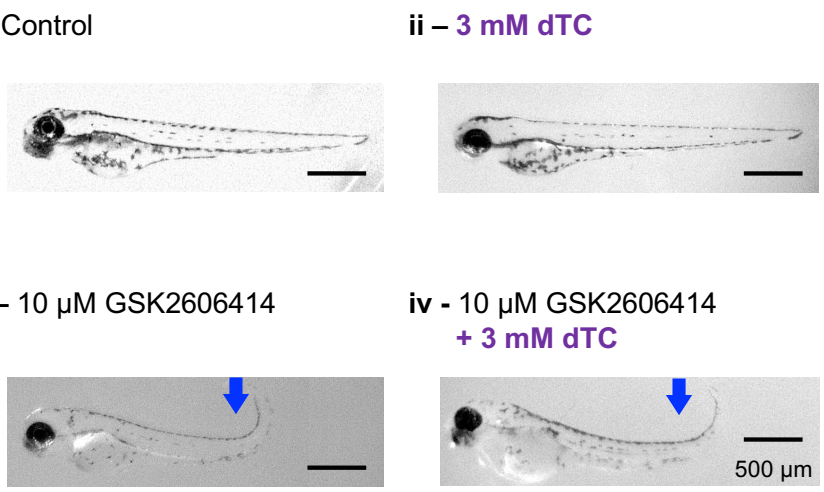

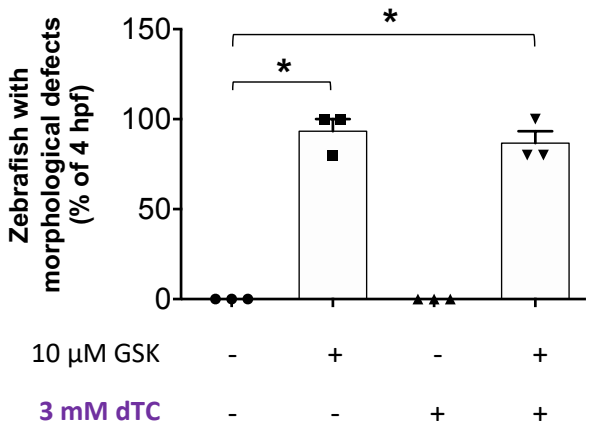

Figure 3

Figure 4

A Pancreatic development

i 28 hpf

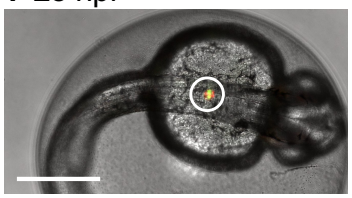

ins:GFP + sst:mCherry

ii 76 hpf

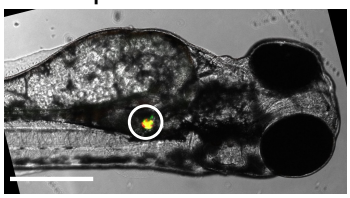

ins:GFP + sst:mCherry

iii 148 hpf

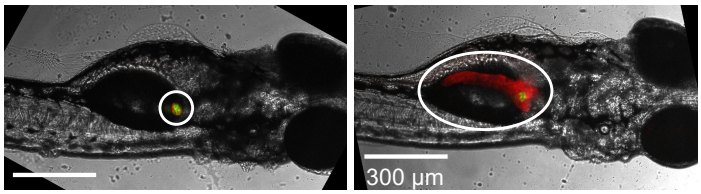

ins:GFP+ sst:mCherry *ins:GFP + ela:mCherry*

B **i** Early (4 hpf) GSK exposure protocol

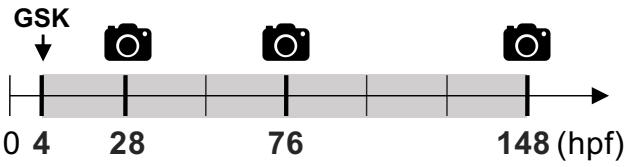

ii Late (76 hpf) GSK exposure protocol

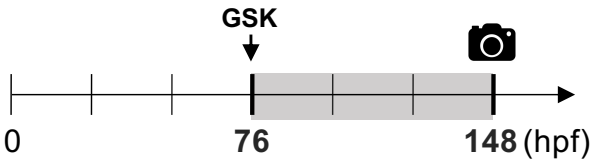

C *ins:GFP* (*β* cell; endocrine)

i Early: 4 hpf → 28 hpf 76 hpf 148 hpf

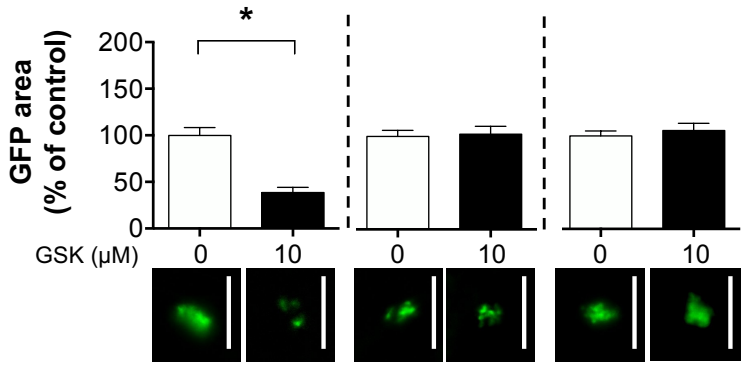

ii Late: 76 hpf → 148 hpf

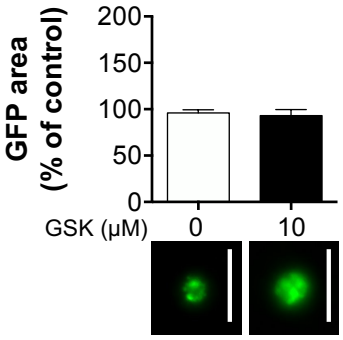

D *sst:mCherry* (*δ* cell; endocrine)

i Early: 4 hpf → 28 hpf 76 hpf 148 hpf

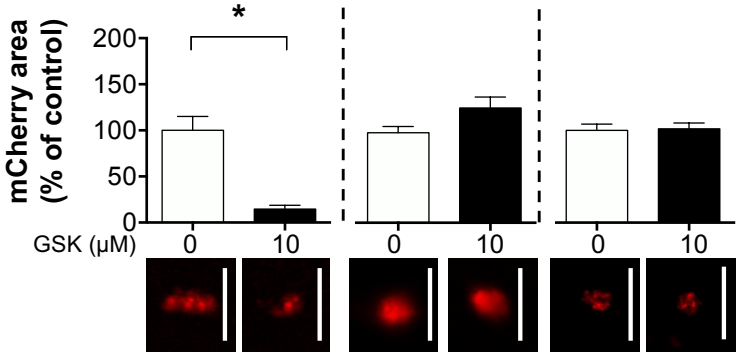

ii Late: 76 hpf → 148 hpf

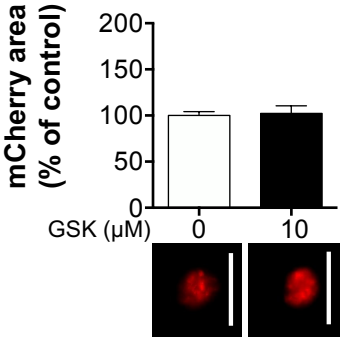

E *ela:mCherry* (exocrine)

i Early: 4 hpf → 148 hpf

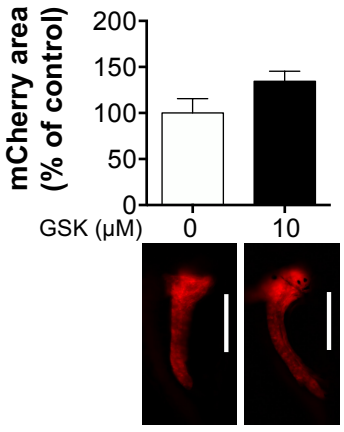

ii Late: 76 hpf → 148 hpf

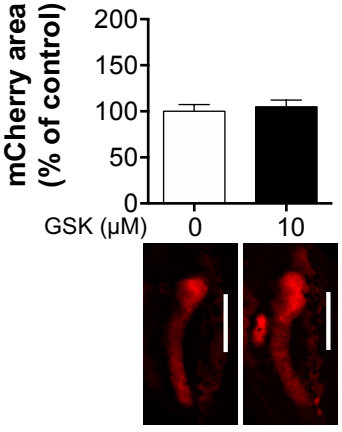

A 2-NBD glucose uptake to neuromasts

i Control

ii 10 μM GSK2606414

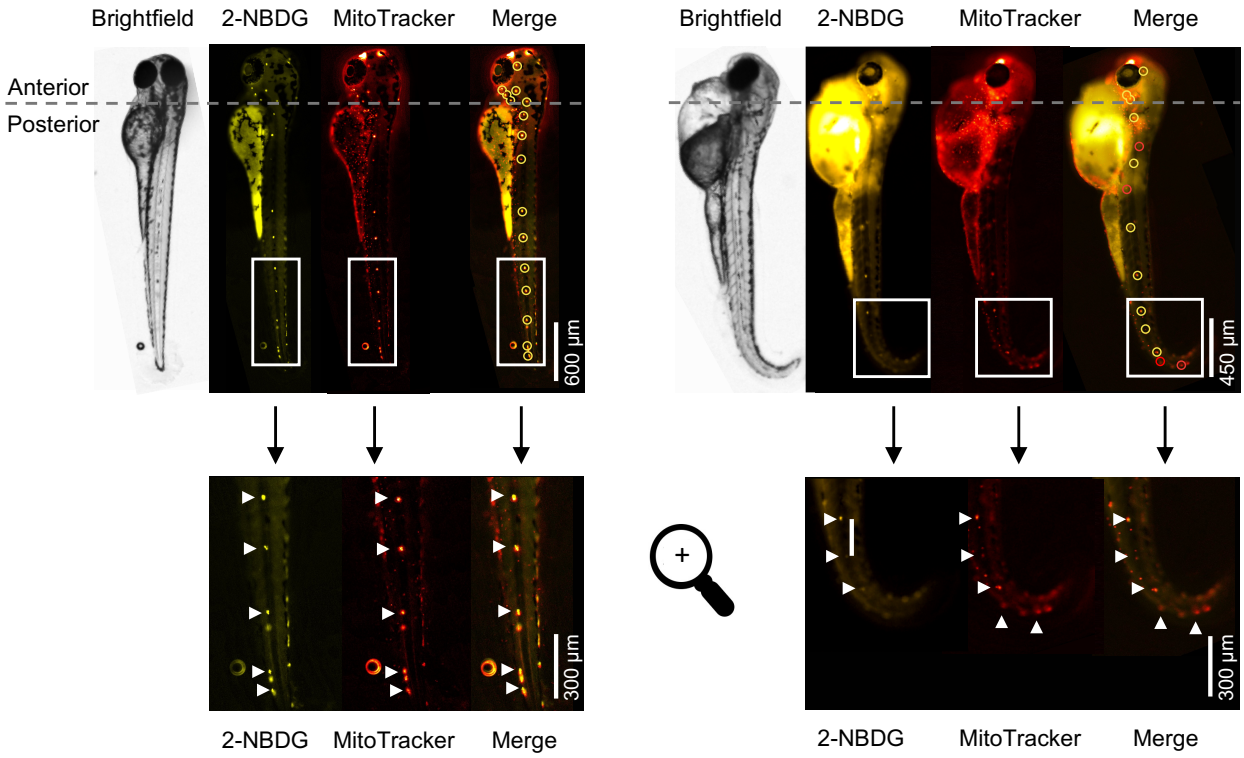

B Neuromast quantification

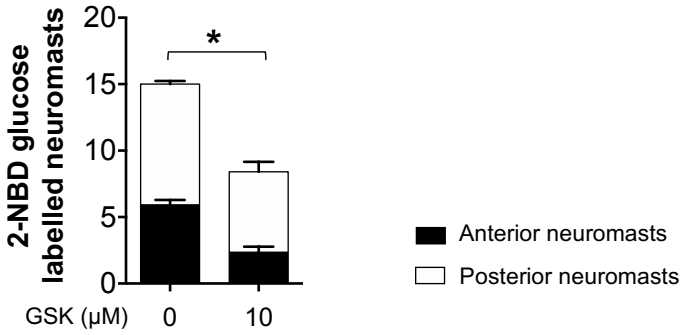

Figure 5

A Tail coiling events (28 hpf)

i

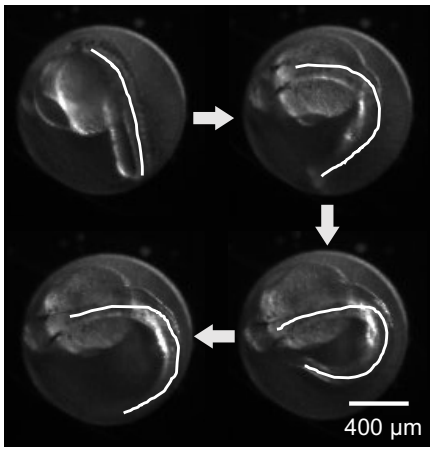

ii

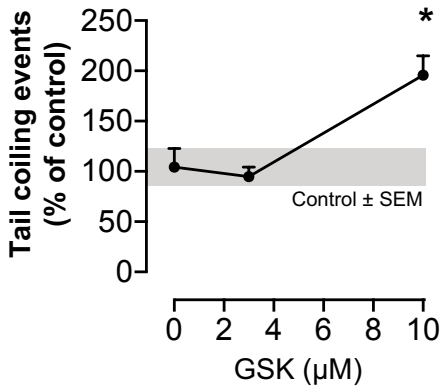

B Touch-evoked escape responses (76 hpf)

i

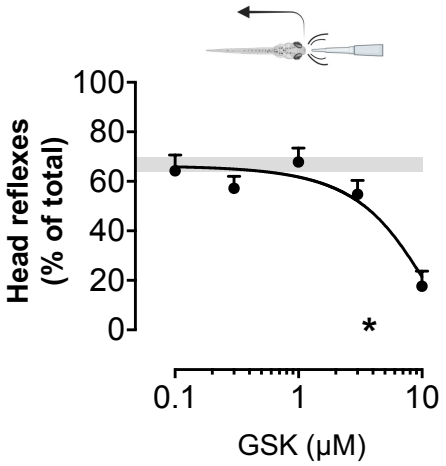

ii

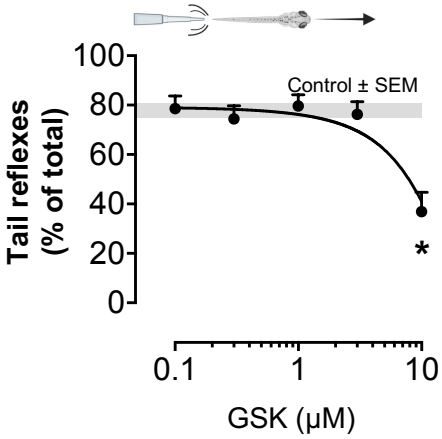

C Birefringence assay (76 hpf)

i

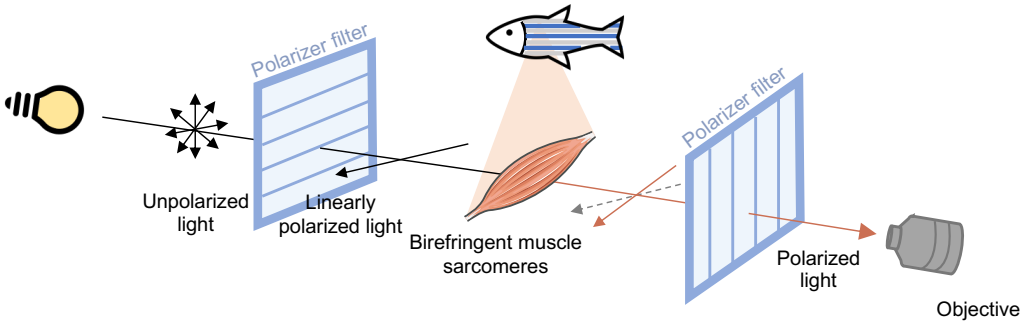

ii

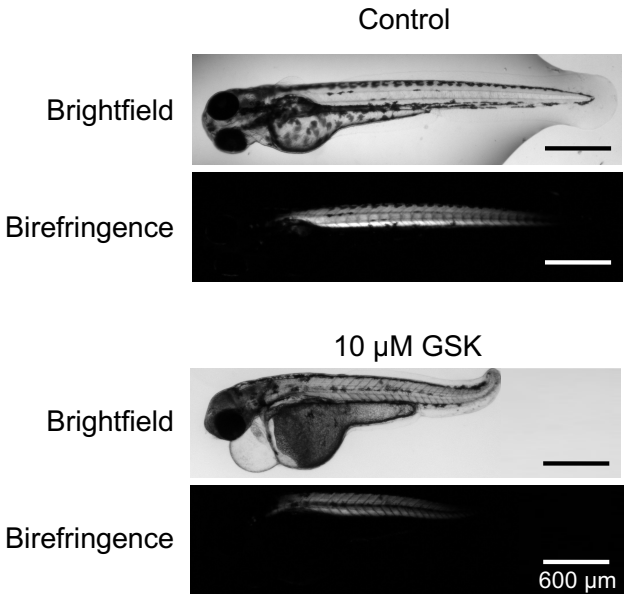

iii

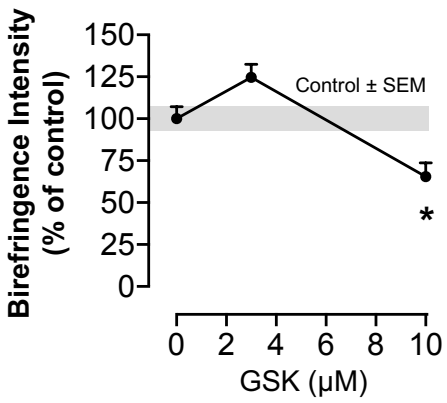

Figure 6

A Pericardial oedema

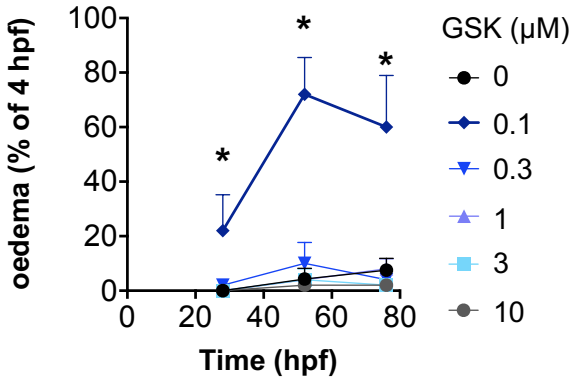

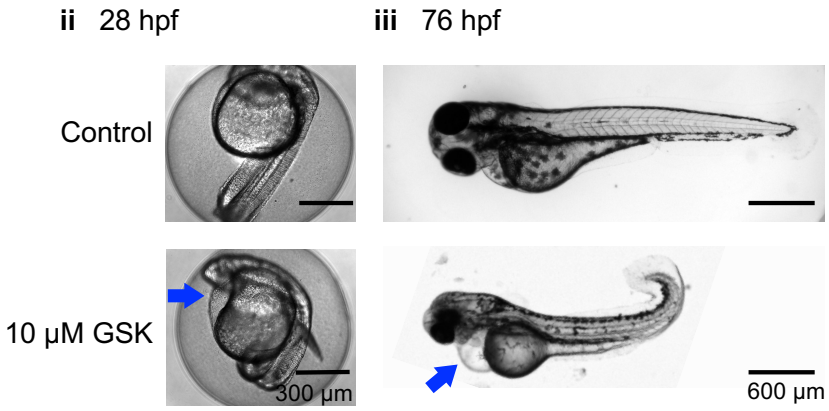

B Heart beat analysis

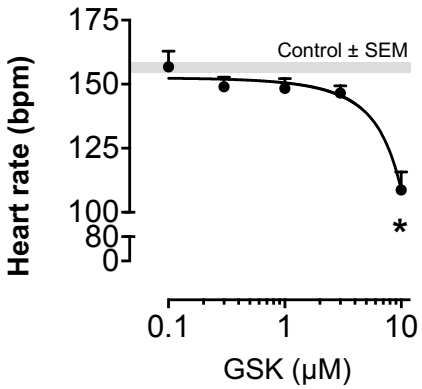

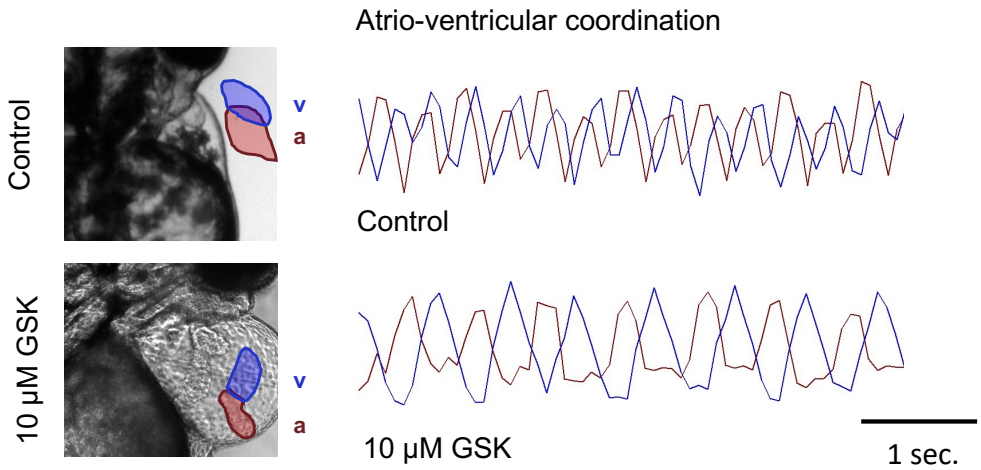

Figure 7

Supplementary Material

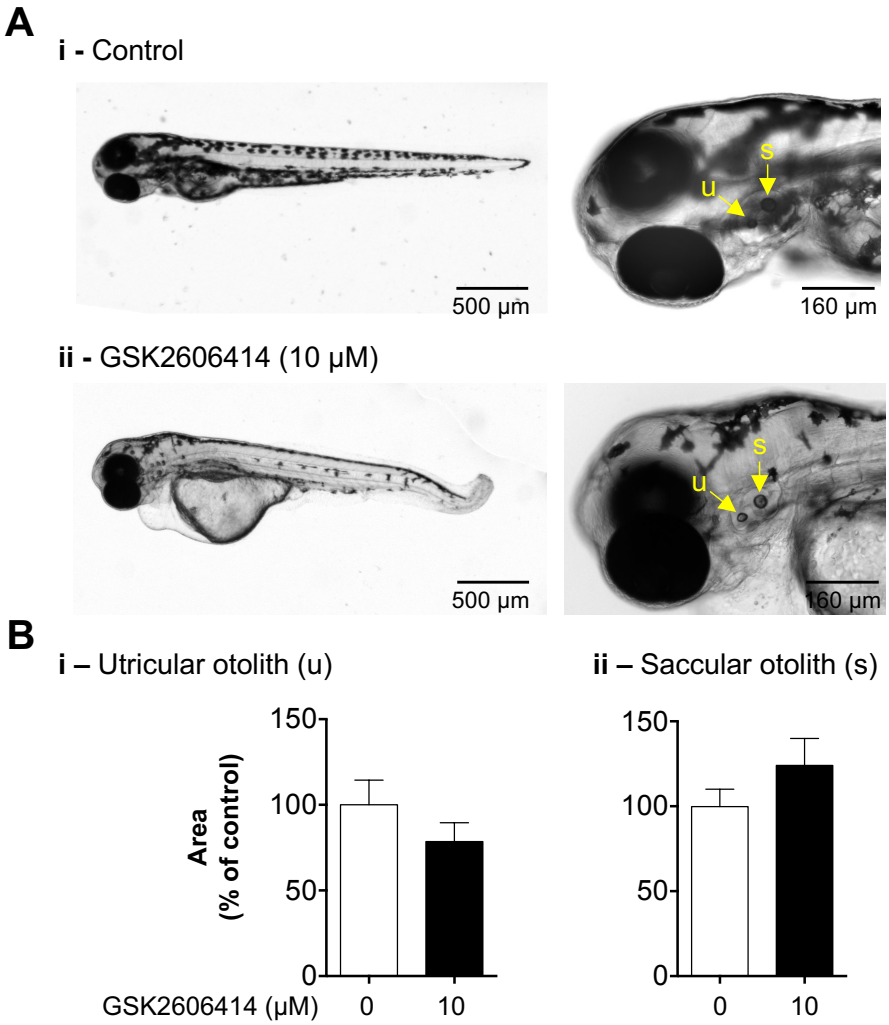

Supplementary Figure 1. GSK2606414 (GSK) does not alter zebrafish otolith area. **(A)** Representative images of zebrafish at 76hpf following treatment with control (0 µM GSK) or 10 µM GSK since 4 hpf. Arrows: (u) utricular/anterior otolith, (s) saccular/posterior otolith. **(B)** Mean ± SEM of the otolith area, $P > 0.05$, t-test, $n = 15$ larvae, 3 zebrafish experiments.

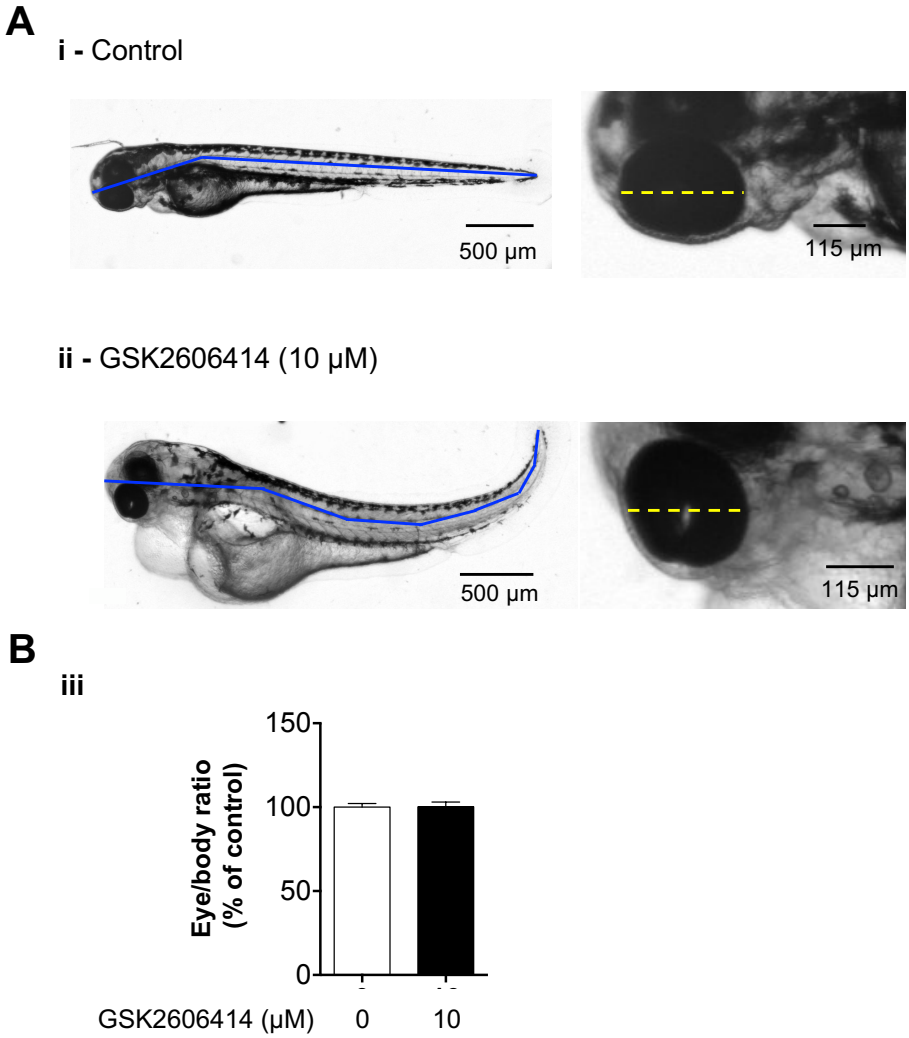

Supplementary Figure 2. GSK2606414 does not alter zebrafish eye/body ratio. **(A)** Representative images of zebrafish at 76hpf following treatment with control (0 µM GSK) or 10 µM GSK since 4 hpf. Solid blue lines: body length; dashed yellow lines: eye diameter. **(B)** Mean ± SEM of the eye/body ratio, $P > 0.05$, t-test, $n = 15$ zebrafish, 3 independent experiments.

Supplementary Table 1. Primary antibodies used in western blots from Fig. 2 D.

Antibody	Dilution	Supplier	Catalog Number	RRID
anti-ATF4	1:500	Proteintech	Cat# 10835-1-AP	AB_2058600
anti-CHOP	1:1000	Proteintech	Cat# 15204-1-AP	AB_2292610
anti-eIF2α	1:1000	Thermo Fisher Scientific	Cat# AHO0802	AB_2536316
anti-p-eIF2α	1:500	Thermo Fisher Scientific	Cat# MA5-15133	AB_10983400

Supplementary Table 2. Secondary antibodies used in western blots from Fig. 2 D.

Antibody	Dilution	Supplier	Catalog Number	RRID
anti-mouse	1:4000	Thermo Fisher Scientific	Cat# G-21040	AB_2536527
anti-rabbit	1:4000	Thermo Fisher Scientific	Cat# G-21234	AB_2536530